



**SPE 161092**

## **A New Approach to Reserves Estimation in Shale Gas Reservoirs Using Multiple Decline Curve Analysis Models**

Srikanta Mishra, SPE, Battelle Memorial Institute

Copyright 2012, Society of Petroleum Engineers

This paper was prepared for presentation at the SPE Eastern Regional Meeting held in Lexington, Kentucky, USA, 3–5 October 2012.

This paper was selected for presentation by an SPE program committee following review of information contained in an abstract submitted by the author(s). Contents of the paper have not been reviewed by the Society of Petroleum Engineers and are subject to correction by the author(s). The material does not necessarily reflect any position of the Society of Petroleum Engineers, its officers, or members. Electronic reproduction, distribution, or storage of any part of this paper without the written consent of the Society of Petroleum Engineers is prohibited. Permission to reproduce in print is restricted to an abstract of not more than 300 words; illustrations may not be copied. The abstract must contain conspicuous acknowledgment of SPE copyright.

### **Abstract**

Recent interest in the development of Marcellus and Utica plays has renewed attention on the problem of reliable estimation of recoverable reserves from low-permeability shale gas formations. Over-optimistic results obtained from the commonly used Arps hyperbolic model has led to the development of alternative decline curve analysis models based on empirical considerations (e.g., Duong's power law model) or mechanistic considerations (e.g., Valko's SEDM). This work addresses the practical difficulty of discriminating between such models (including a new mechanistic model proposed for decline curve analysis based on the Weibull growth curve) from limited production data. The paper also presents a new approach to aggregating estimated ultimate recovery (EUR) forecasts from multiple plausible models using the Generalized Likelihood Uncertainty Estimation (GLUE) methodology.

Two field examples are presented to demonstrate the performance of Hyperbolic, SEDM, Duong and Weibull models. Model parameters are estimated via nonlinear regression using Excel-SOLVER, from which 30-year EUR estimates are generated. The GLUE procedure is then used for determining the likelihood of each model by weighting the results with  $[1/\text{RMSE}^2]$ , and computing the weighted mean and standard deviation for the 30-year EUR. For the first example (with 15 years of data), excellent visual fits are obtained for both rate and cumulative production with all four models. However, 30-year EUR estimates from the Arps and Duong models are on the high side and the SEDM and Weibull models are on the low side. The uncertainty in the mean amounts to only ~2%. For the second example (with 52 months of data), the trends are very similar, albeit with greater separation in the 30-year EUR forecasts and a higher uncertainty in the mean EUR (~7%).

These results reinforce earlier findings that multiple alternative models can provide equally good fits to limited-duration production data, but yield very different 30-year EUR forecasts. The GLUE approach provides a robust methodology for aggregating such analyses and quantifying the uncertainty of the EUR forecast.

### **Introduction**

The introduction of horizontal drilling supplemented by multi-stage hydraulic fracturing has spurred the production of shale gas from "unconventional" gas plays. These include the Barnett, Eagleford, Haynesville, Marcellus, and most recently, the Utica shale plays. This growing interest in the exploitation of shale gas has also brought forth many challenges in production forecasting and reserves estimation.

As noted by Lee and Sidle (2010), projection of production decline curves is perhaps the single most widely used method for forecasting future production from tight gas and shale gas wells. Future production potential at any given time, and estimated ultimate recovery (EUR) are estimated by: (a) fitting an empirical model of the trend in production decline from the well's history, and (b) projecting this trend into the future to terminate at the well's economic limit or a common cutoff time, e.g., 30-years. The most commonly used production decline curve model is the Arps' Hyperbolic model (Arps, 1945). However, force-fitting of the Hyperbolic model to production data from shale gas wells has often been found to result in over-optimistic results for the EUR stemming from physically unrealistic high values fitted to the decline exponent (Lee and Sidle, 2010). This quandary has resulted in several alternatives being proposed for analyzing decline curves from tight gas wells. One approach involves constraining the late-time decline rate to something more realistic based on experience and/or analogs. The other approach involves searching for alternative empirical decline curve models that impose physically meaningful parameter definitions and finite EUR values on model predictions. A key issue associated with the use of multiple models is how to discriminate between them based on data from limited production periods, and how to combine the model results to yield an assessment of uncertainty in reserve estimates.

Two recently postulated empirical models have been highlighted as useful alternatives to the Hyperbolic model (Lee, 2012), viz: the Stretched Exponential Decline Model (Valko, 2009), and the Duong power law model (Duong, 2011). In addition, the Weibull growth curve (Tabatabai et al., 2005) offers promise for modeling production decline curves based on its performance in modeling growth kinetics for biologic phenomena. The first objective of this paper is therefore to provide a comparison of the performance of these models for two field examples. Next, an uncertainty quantification framework for aggregating model results using the Generalized Likelihood Uncertainty Estimation (GLUE) methodology will be described and applied for the two field examples.

The paper begins with an overview of the formulation for the four empirical decline curve models of interest, i.e., Hyperbolic, SEDM, Duong and Weibull. This is followed by an overview of the proposed uncertainty assessment protocol using statistical model averaging concepts. Next, the procedures for fitting decline curves and aggregating model results are applied to two field data sets. Finally, some conclusions based on this study are presented.

## Review of Decline Curve Analysis Models

### Arps' Hyperbolic Model

In the Hyperbolic model, the production rate declines with time according to the following relationship:

$$q = q_i \frac{1}{(1 + bD_i t)^{(1/b)}} \quad (1)$$

where  $q$  is the time-varying production rate,  $q_i$  is the initial production rate parameter,  $b$  is the hyperbolic decline exponent parameter  $0 < b < 1$ , and  $D_i$  is the initial decline rate parameter. Integration of Eq. (1) leads to an expression for cumulative production,  $G_p$ :

$$G_p = \frac{q_i^b}{D_i(b-1)} \left( q(t)^{(1-b)} - q_i^{(1-b)} \right) \quad (2)$$

Analysis of production decline from tight gas and shale gas wells using Eq. (1) typically results in a best-fit value of greater than unity for the decline exponent parameter,  $b$  (Lee and Sidle, 2010). This leads to the physically unrealistic result that cumulative production becomes unbounded as time increases, as can be seen from the following:

$$\lim_{t \rightarrow \infty} G_p = \frac{q_i^b}{D_i(b-1)} \left( \frac{1}{q(t)^{(b-1)}} - \frac{1}{q_i^{(b-1)}} \right) \rightarrow \infty \quad (3)$$

Fetkovich et al. (1987) have argued that such anomalous behavior, i.e., values of  $b > 1$  in Eq. (1) or Eq. (2), arises when data from the transient-flow period are used to fit a model that is only appropriate during boundary-dominated flow. Supporting this assertion is the observation that best-fit  $b$  values that start out being greater than unity tend to decrease with time as more and more data become available (e.g., Blasingame and Rushing, 2005). However, the use of the Hyperbolic model continues to remain popular for reserves estimation purposes. A heuristic approach to keeping the long-term reserve estimates finite, with best-fit  $b$  values  $> 1$ , involves switching to an exponential decline with a prescribed minimum decline rate based on analogy or intuition (Harrell et al., 2004).

### Stretched Exponential Decline Model (SEDM)

In order to avoid the arbitrariness associated with long-term reserve estimates from the Hyperbolic model, Valko (2009) proposed the SEDM, where production rate declines with time according to the following relationship:

$$q = q_0 \exp \left[ - \left( \frac{t}{\tau} \right)^n \right] \quad (4)$$

where  $q$  is the time-varying production rate,  $q_0$  is the initial production rate parameter,  $\tau$  is the characteristic time parameter, and  $n$  is the exponent parameter. Integration of Eq. (4) leads to an expression for cumulative production,  $G_p$ :

$$G_p = \frac{q_0 \tau}{n} \left\{ \Gamma \left[ \frac{1}{n} \right] - \Gamma \left[ \frac{1}{n}, \left( \frac{t}{\tau} \right)^n \right] \right\} \quad (5)$$

where  $\Gamma$  is the incomplete Gamma function (Abramowitz and Stegun, 1972).

The SEDM model can be interpreted as the cumulative effect of multiple contributing volumes in exponential decay, but with different characteristic time constants (Valko, 2010). Valko argues that this is a more plausible physical explanation

than the assumption of boundary-dominated flow – which may take extremely long times to develop in tight and shale gas reservoirs – required justifying the use of the Hyperbolic model. Another benefit of the SEDM is that unlike the Hyperbolic model, it yields a finite value for ultimate recovery given positive values of  $n$ ,  $\tau$  and  $q_0$ . As Lee (2012) has indicated, SEDM appears to fit field data from various shale plays quite well, and provides an effective alternative to Arps Hyperbolic model.

### Duong Model

Since tight gas and shale gas reservoirs are generally produced after massive hydraulic fracturing, it is reasonable to assume that flow to wells in such systems will exhibit typical fracture-dominated characteristics. For finite conductivity fractures, the flow will be bilinear which manifests as a quarter-slope line on a log-log plot of production rate v/s time, whereas for infinite conductivity fractures, flow will be linear and characterized by a half slope line on the same plot (Kamal, 2009). Under both conditions, Duong (2011) has shown that a log-log plot of  $q/G_p$  versus time should have a slope of -1. However, analysis of field data from several shale gas plays has shown that in reality, the relationship between these variable is better described using the following empirical form:

$$\frac{q}{G_p} = at^{-m} \quad (6)$$

where  $a$  is the intercept constant and  $m$  is the slope parameter. The slope is negative, but  $m$  is always positive and greater than unity for shale gas reservoirs (based on field data). Duong (2011) derived expressions for production rate and cumulative production v/s time that satisfy Eq. (6) as given below:

$$q = q_1 t^{-m} \exp\left(\frac{a}{1-m}(t^{1-m} - 1)\right) \quad (7)$$

$$G_p = \frac{q_1}{a} \exp\left(\frac{a}{1-m}(t^{1-m} - 1)\right) \quad (8)$$

As Lee (2012) has indicated, Duong's empirical model also appears to fit field data from various shale plays quite well, and provides an effective alternative to Arps Hyperbolic model.

### Weibull Growth Model

The analysis of growth (or decline) forms a key element of many biological and clinical studies. Many mathematical functions have been used to effectively describe population growth (or decline) under a wide range of conditions (Kingland, 1982). Some of the popular models include the Gompertz, Richards, logistic and Weibull models (Zeide, 1993). The logistic model has also been used for analyzing decline curve data for unconventional gas wells (Clark, 2011). However, Tabatabai et al. (2011) note that the Weibull model performs much better than the logistic model to accurately predict and analyze self-limited growth behavior. In this study, the application of the Weibull model is explored in detail for analyzing production decline curves and forecasting reserves.

The Weibull growth curve is a generalization of the widely used Weibull distribution for modeling time-to-failure in applied engineering problems (Weibull, 1954), and is expressed as:

$$P(t) \equiv G_p = M \left\{ 1 - \exp\left[-\left(\frac{t}{\alpha}\right)^\gamma\right] \right\} \quad (9)$$

where  $P(t)$  is the cumulative growth,  $M$  is the carrying capacity,  $\alpha$  is the scale parameter and  $\gamma$  is the shape parameter. The cumulative growth,  $P(t)$ , can be equated to cumulative gas production,  $G_p$ . Carrying capacity,  $M$ , is the physical growth (production) limit for the system, and provides an upper bound on resource extraction – unlike the Hyperbolic model. The scale parameter,  $\alpha$ , is that value of time at which  $(1-1/e)$  or 63.2% of the resources have been (or will be) produced. The shape parameter,  $\gamma$ , describes how the rate of growth changes with time. In unconventional gas wells,  $\gamma$  will typically be less than 1, indicating that the rate of growth is declining with time.

The instantaneous rate of growth is readily obtained by differentiating Eq. (9):

$$p(t) \equiv q = M \frac{\gamma}{\alpha} \left(\frac{t}{\alpha}\right)^{\gamma-1} \exp\left[-\left(\frac{t}{\alpha}\right)^\gamma\right] \quad (10)$$

In terms of parameter estimation, note that the three-parameter Weibull model is reduced to 2 unknowns if we take the ratio of production rate,  $q$ , and cumulative production,  $G_p$ , as the dependent variable. Nonlinear regression analysis can then be used to estimate observed  $q/G_p$  v/s time to the ratio of Eq. (10 and Eq. (9). In the next step,  $M$  can be estimated from fitting cumulative production data to Eq. (9).

### Uncertainty Assessment using Model Averaging

Previous studies of decline curve analysis using multiple models have shown that fits of comparable quality can be obtained for short data windows, but will produce very different 30-year EUR estimates (e.g., Valko, 2010). To our knowledge, a formal approach for discriminating among such models using goodness-of-fit statistics (or any equivalent measure) does not appear to have been discussed in the shale gas literature. Furthermore, if multiple models are indeed to be used for generating reserves estimates, it is not clear how the results from such models can be aggregated. To this end, this study proposes a two-step approach based on related work on “model averaging” carried out in the context of hydrologic modeling (Beven and Binley, 1992; Neuman, 2003; Singh et al., 2010). In the first step, alternative models are identified and used to fit the data. In the second step, a weight is assigned to each model based on some goodness-of-fit statistics, and weighted mean and standard deviation of the desired performance measure (i.e., 30-year EUR) are calculated.

Two commonly used model averaging techniques for hydrologic modeling are Generalized Likelihood Uncertainty Estimation or GLUE (Beven and Binley, 1992), and Maximum Likelihood Bayesian Model Averaging or MLBMA (Neuman, 2003). Singh et al. (2010) have compared the performance of the heuristic GLUE approach to the more formal MLBMA techniques. They observed that the Bayesian model averaging approach tends to concentrate model weights on only 1-2 best performing models, whereas model weights calculated by GLUE are more uniformly distributed across the model space. In what follows, details of the GLUE methodology will be presented to demonstrate how results from different plausible models can be aggregated.

GLUE was originally proposed for dealing with model non-uniqueness in hydrologic catchment modeling. It is based on the concept of ‘equifinality’, i.e., the possibility that the same final state may be obtained from a variety of initial states (Beven and Binley, 1992). In other words, a single set of observed data may be (non-uniquely) matched by multiple parameter sets that produce similar model predictions. The GLUE framework accepts many equally likely parameter combinations (realizations) or distinct model alternatives as a starting point. The output corresponding to each realization (or model alternative) is compared against actual observations. Only those realizations (or models) that satisfy some acceptable level of performance (e.g. a maximum sum-of-squared-weighted-residuals), also known as the behavioral threshold, are retained for further analysis, and the non-behavioral realizations (models) are rejected. A “likelihood” for each model is then computed as a function of the misfit between observations and model predictions. The weights (or probabilities) for each model are estimated by normalizing the likelihoods.

One of the central features of GLUE is the flexibility with respect to the choice of the likelihood measure. As the name “generalized likelihood” implies, any reasonable likelihood measure can be used appropriately as long as it adequately represents the experts’ understanding of the relative importance of different data sources used to assess model accuracy. In the literature, many different likelihood measures based on goodness-of-fit metrics have been proposed. One likelihood measure that has seen widespread usage in the GLUE literature is given by the inverse weighted variance:

$$L_j = \left( \frac{\sigma_o^2}{\sigma_{e,j}^2} \right)^N \quad (11)$$

where  $L_j$  is the likelihood for model  $j$ ,  $\sigma_{e,j}^2$  is the variance of the errors (residuals) for model  $j$ ,  $\sigma_o^2$  is the variance of the observations, and  $N$  is a shape factor such that values of  $N \gg 1$  tend to give higher weights (likelihoods) to models with better agreement with the data, and values of  $N \ll 1$  tend to make all models equally likely. A simpler version of Eq. (11) can be defined using the traditional root-mean-square-error (RMSE) statistic as follows:

$$L_j \propto \left( \frac{1}{RMSE} \right)^2 \quad (12)$$

Normalizing the likelihoods, so that their sum is equal to one, gives the GLUE weight for each model:

$$w_j(GLUE) = \frac{Pr_j L_j}{\sum_{j=1}^n Pr_j L_j} = \frac{Pr_j / (RMSE)^2}{\sum_{j=1}^n Pr_j / (RMSE)^2} \quad (13)$$

where  $L_j$  is the likelihood functions described above in Eq. (11),  $Pr_j$  is the prior weight given to each model (i.e.,  $1/n$  if all are assumed equally likely prior to weighting), and  $n$  is the total number of models being considered. From these weights, the aggregated 30-year EUR across the model ensemble (i.e., weighted average) can be computed from:

$$G_{p,30}(avg) = \sum_{j=1}^n w_j G_{p,30} |_{j} \quad (14)$$

and the standard deviation can be computed from

$$SD[G_{p,30}] = \sqrt{\sum_{j=1}^n w_j \left\{ G_{p,30}(avg) - G_{p,30}|_j \right\}^2} \quad (15)$$

### Field Examples

Two field examples are presented from unconventional shale gas reservoirs to provide a comparative assessment of various decline curve analysis models, and to quantify the uncertainty associated with 30-year EUR estimates. These examples will be first analyzed using the four decline curve analysis models described earlier, viz., Arps' Hyperbolic model, Stretched Exponential Decline Model (SEDM), Duong model and Weibull model to estimate the 30-year EUR. Next, goodness-of-fit statistics from these model fits will be used to compute a likelihood or weighting factor for each model using the GLUE methodology. These weights will then be used to aggregate the individual model forecasts.

#### Example – 1

The first example is taken from a 15-year dataset presented as Example 3 in the rate/time analysis spreadsheet developed at Texas A&M University (Ilk et al., 2008). During this period, the production declined from ~850 MSCF/d to ~35 MSCF/d, resulting in a cumulative production of ~0.45 BCF.

**Arps' Hyperbolic Model:** For the Arps' Hyperbolic model, the first step is to fit the ratio of observed production rate,  $q$ , and cumulative production,  $G_p$ , to the model (i.e., ratio of  $q/G_p$  from Eq. 1 and 2) to estimate the decline exponent,  $b$ , and the initial decline rate,  $D_i$ , using Microsoft Excel's Solver add-in. The resulting fit, shown in **Fig. 1**, appears to capture the trend in the data very well, excepting for the downward trend at the very end of the data. The resulting best fit parameters are  $b = 1.82$  and  $D_i = 0.109$  1/d. In the next step, the initial production rate,  $q_i$ , is calculated by fitting the observed  $G_p$  data to Eq. 2, with an excellent agreement as shown in **Fig. 2**. The resulting best fit parameter is  $q_i = 1.85E3$  MSCF/d. **Fig. 3** compares the observed production rate,  $q$ , with that obtained using the best fit parameters in Eq. 1. As in **Fig. 1**, the agreement is very good excepting at the very end of the data record. Using these fitted parameters, the 30-year production rate,  $q_{30}$ , is estimated to be 27.1 MSCF/d, and the 30-year cumulative production (30-year EUR),  $G_{p,30}$ , is estimated to be 6.39E5 MSCF.

**SEDM:** For the Stretched Exponential Decline model, the first step is to fit the ratio of observed production rate,  $q$ , and cumulative production,  $G_p$ , to the model (i.e., ratio of  $q/G_p$  from Eqn. 4 and 5) to estimate the characteristic time parameter,  $\tau$ , and the exponent parameter,  $n$ , using Microsoft Excel's Solver add-in. The resulting best fit parameters are  $\tau = 8.52E-2$  months and  $n = 0.144$ . In the next step, the initial production rate parameter,  $q_0$ , is calculated by fitting the observed  $G_p$  data to Eq. 5, with an excellent agreement as shown in **Fig. 4**. The resulting best fit parameter is  $q_0 = 5.00E3$  MSCF/d. **Fig. 5** compares the observed production rate,  $q$ , with that obtained using the best fit parameters in Eq. 4. As in **Fig. 3**, the agreement is very good excepting at the very end of the data record. Using these fitted parameters, the 30-year production rate,  $q_{30}$ , is estimated to be 22.2 MSCF/d, and the 30-year cumulative production (30-year EUR),  $G_{p,30}$ , is estimated to be 6.14E5 MSCF.

**Duong Model:** For the Duong model, the first step is to fit the ratio of observed production rate,  $q$ , and cumulative production,  $G_p$ , to the empirical model postulated by Duong in Eq. 6 to estimate the intercept constant,  $a$ , and the slope parameter,  $m$ , using Microsoft Excel's Solver add-in. The resulting fit, shown in **Fig. 6**, appears to capture the trend in the data very well, excepting for the downward trend at the very end of the data. The corresponding best fit parameters are  $a = 0.764$  1/d and  $m = 1.06$ . In the next step, the theoretical rate at day 1,  $q_1$ , is calculated by performing a linear regression of the observed production rate,  $q$ , against the time function  $f(a,t)$ , which is the RHS of Eq. 7. The resulting best fit parameter, based on **Fig. 7**, is  $q_1 = 2.03E3$  MSCF/d. **Fig. 8** compares the observed production rate,  $q$ , with that obtained using the best fit parameters in Eq. 7. As in **Fig. 3**, the agreement is very good excepting at the very end of the data record. **Fig. 9** compares the cumulative production,  $G_p$ , with that obtained using the best fit parameters in Eq. 8 – showing an excellent agreement. Using these fitted parameters, the 30-year production rate,  $q_{30}$ , is estimated to be 25.4 MSCF/d, and the 30-year cumulative production (30-year EUR),  $G_{p,30}$ , is estimated to be 6.30E5 MSCF.

**Weibull Model:** For the Weibull model, the first step is to fit the ratio of observed production rate,  $q$ , and cumulative production,  $G_p$ , to the model (i.e., ratio of  $q/G_p$  from Eq. 8 and 9) to estimate the shape parameter,  $\alpha$ , and the scale parameter,  $\gamma$ , using Microsoft Excel's Solver add-in. The resulting fit, shown in **Fig. 10**, appears to capture the trend in the data very well, excepting for the downward trend at the very end of the data. The resulting best fit parameters are  $\alpha = 1.68E4$  and  $\gamma = 0.577$ . In the next step, the "carrying capacity",  $M$ , is calculated by fitting the observed  $G_p$  data to Eq. 9, with an excellent agreement as shown in **Fig. 11**. The resulting best fit parameter is  $M = 1.13E6$  MSCF. **Fig. 12** compares the observed production rate,  $q$ , with that obtained using the best fit parameters in Eq. 8. As in **Fig. 10**, the agreement is very good

excepting at the very end of the data record. Using these fitted parameters, the 30-year production rate,  $q_{30}$ , is estimated to be 21.3 MSCF/d, and the 30-year cumulative production (30-year EUR),  $G_{p,30}$ , is estimated to be 6.12E5 MSCF.

**Aggregation of Results:** Fig. 13 shows an overlay of 30-year production rate forecasts from each of these 4 models. As has been discussed previously, the models honor the trend of the data very well excepting at the end of the data record, i.e., around 180 months. The 30-year forecast show that the Hyperbolic model yields the most optimistic projection, followed by the Duong model, SEDM and the Weibull model. These trends are also reinforced in the overlay for the cumulative production shown in Fig. 14 (albeit with much less data scatter). Table 1 shows the RMSE corresponding to the  $G_p$  fit for each of the models, and the likelihood (model weight) calculated using the GLUE approach, viz., Eq. 12. The Weibull model has the lowest RMSE, and hence, the highest weight at 39.7%. The weights for the other models are 27.6% for SEDM, 22.2% for the Duong model and 10.6% for the Hyperbolic model. Using Eq. 13, the weighted mean for 30-year EUR estimates can then be calculated as 6.20E5 MSCF with a weighted standard deviation of 9.72E3 MSCF, i.e., a coefficient of variation of 1.57%.

### Example – 2

The second example corresponds to the 52 month field-averaged data from 237 wells in Denton County, TX, used in a recent SPE webinar presentation (Lee, 2012). During this period, the production declined from ~8E6 MSCF/d to ~1.6E6 MSCF/d, with a cumulative production of ~ 160 BCF.

**Arps Hyperbolic Model:** For the Arps Hyperbolic model, the first step is to fit the ratio of observed production rate,  $q$ , and cumulative production,  $G_p$ , to the model (i.e., ratio of  $q/G_p$  from Eq. 1 and 2) to estimate the decline exponent,  $b$ , and the initial decline rate,  $D_i$ , using Microsoft Excel's Solver add-in. The resulting fit, shown in Fig. 15, captures the trend in the data very well. The resulting best fit parameters are  $b = 1.46$  and  $D_i = 0.121$  1/d. In the next step, the initial production rate,  $q_i$ , is calculated by fitting the observed  $G_p$  data to Eq. 2, with an excellent agreement as shown in Fig. 16. The resulting best fit parameter is  $q_i = 8.30E6$  MSCF/d. Fig. 17 compares the observed production rate,  $q$ , with that obtained using the best fit parameters in Eq. 1. As in Fig. 15, the agreement is very good. Using these fitted parameters, the 30-year production rate,  $q_{30}$ , is estimated to be 4.79E5 MSCF/d, and the 30-year cumulative production (30-year EUR),  $G_{p,30}$ , is estimated to be 4.07E8 MSCF.

**SEDM:** For the Stretched Exponential Decline model, the first step is to fit the ratio of observed production rate,  $q$ , and cumulative production,  $G_p$ , to the model (i.e., ratio of  $q/G_p$  from Eq. 4 and 5) to estimate the characteristic time parameter,  $\tau$ , and the exponent parameter,  $n$ , using Microsoft Excel's Solver add-in. The resulting best fit parameters are  $\tau = 1.62$  months and  $n = 0.276$ . In the next step, the production parameter,  $q_0$ , is calculated by fitting the observed  $G_p$  data to Eq. 5, with excellent agreement as shown in Fig. 18. The resulting best fit parameter is  $q_0 = 2.20E7$  MSCF/d. Fig. 19 compares the observed production rate,  $q$ , with that obtained using the best fit parameters in Eq. 4, showing very good agreement. Using these fitted parameters, the 30-year production rate,  $q_{30}$ , is estimated to be 2.52E5 MSCF/d, and the 30-year cumulative production (30-year EUR),  $G_{p,30}$ , is estimated to be 3.46E8 MSCF.

**Duong Model:** For the Duong model, the first step is to fit the ratio of observed production rate,  $q$ , and cumulative production,  $G_p$ , to the empirical model postulated by Duong in Eq. 6 to estimate the intercept constant,  $a$ , and the slope parameter,  $m$ , using Microsoft Excel's Solver add-in. The resulting fit, shown in Fig. 20, appears to capture the trend in the data very well. The corresponding best fit parameters are  $a = 1.06$  and  $m = 1.17$ . In the next step, the theoretical rate at day 1,  $q_1$ , is calculated by performing a linear regression of the observed production rate,  $q$ , against the time function  $f(a,t)$ , which is the RHS of Eqn. 7. The resulting best fit parameter, based on Fig. 21, is  $q_1 = 8.07E6$  MSCF/d. Fig. 22 compares the observed production rate,  $q$ , with that obtained using the best fit parameters in Eq. 7, showing excellent agreement. Fig. 23 compares the cumulative production,  $G_p$ , with that obtained using the best fit parameters in Eq. 8 – also showing an excellent agreement. Using these fitted parameters, the 30-year production rate,  $q_{30}$ , is estimated to be 4.25E5 MSCF/d, and the 30-year cumulative production (30-year EUR),  $G_{p,30}$ , is estimated to be 3.92E8 MSCF.

**Weibull Model:** For the Weibull model, the first step is to fit the ratio of observed production rate,  $q$ , and cumulative production,  $G_p$ , to the model (i.e., ratio of  $q/G_p$  from Eqn. 9 and 10) to estimate the shape parameter,  $\alpha$ , and the scale parameter,  $\gamma$ , using Microsoft Excel's Solver add-in. The resulting fit, shown in Fig. 24, appears to capture the trend in the data very well. The resulting best fit parameters are  $\alpha = 89.5$  and  $\gamma = 0.765$ . In the next step, the "carrying capacity",  $M$ , is calculated by fitting the observed  $G_p$  data to Eq. 10, with excellent agreement as shown in Fig. 25. The resulting best fit parameter value is  $M = 3.34E8$  MSCF. Fig. 26 compares the observed production rate,  $q$ , with that obtained using the best fit parameters in Eq. 8, showing excellent agreement as before. Using these fitted parameters, the 30-year production rate,  $q_{30}$ , is estimated to be 1.13E5 MSCF/d, and the 30-year EUR,  $G_{p,30}$ , is estimated to be 3.15E8 MSCF.

**Aggregation of Results:** Fig. 27 shows an overlay of 30-year production rate forecasts from each of these 4 models. As has been discussed previously, the models honor the trend of the data very well. The 30-year forecast shows that the Hyperbolic model yields the most optimistic projection, followed by the Duong model, SEDM and the Weibull model – which is identical to the relative order observed in the previous example. These trends are also reinforced in the overlay for the cumulative production shown in Fig. 28. Note also the large spread in the forecasts because the forecasting period is roughly 7 times that of the data window (360 months v/s 52 months) compared to the previous example, where the forecasting period was only 2 times that of the data window (360 months v/s 180 months). Table 2 shows the RMSE corresponding to the  $G_p$  fit for each of the models, and the likelihood (model weight) calculated using the GLUE approach, viz., Eqn. 10. The Duong model has the lowest RMSE, and hence, the highest weight at 61.0%. The weights for the other models are 18.2% for SEDM, 12.6% for the Duong model and 8.2% for the Weibull model. Using Eqn. 12, the weighted mean for 30-year EUR estimates can then be calculated as 3.79E8 MSCF with a weighted standard deviation of 2.72E7 MSCF, i.e., a coefficient of variation of 7.17%.

## Conclusions

1. A new flexible model with physically meaningful parameters, i.e., the Weibull growth model, has been proposed for decline curve analysis from shale gas reservoirs.
2. An approach to uncertainty assessment of reserves estimates via aggregation of model results using the GLUE methodology has been presented. Here, the RMSE statistic is used to assign likelihoods or weighting factors to the different model under consideration.
3. Two different case studies are presented to demonstrate that multiple decline curve analysis models can result in equally acceptable fits to historical data but yield (potentially) significantly different forecasts,
4. Application of the GLUE methodology provides a simplified approach to uncertainty assessment due to multiple plausible models and aggregation of model results.
5. A systematic framework for decline curve analysis should include: (a) use of multiple models, (b) checking for robustness of parameter estimates and EUR predictions, and (c) using RMSE-based weighting to assess uncertainty in reserves estimates.

## Nomenclature

|            |  |
|------------|--|
| $a$        | = intercept constant in Duong model, 1/d                               |
| $b$        | = Arps hyperbolic decline exponent, dimensionless                      |
| $D_i$      | = Initial decline rate, 1/d  |
| $G_p$      | = cumulative gas production, MSCF                                      |
| $G_{p,30}$ | = cumulative gas production at 30-years (EUR), MSCF                    |
| EUR        | = Expected Ultimate Recovery, MSCF                                     |
| $L$        | = likelihood, dimensionless  |
| $m$        | = slope parameter in Duong model, dimensionless                        |
| $M$        | = carrying capacity in Weibull model, MSCF                             |
| $n$        | = exponent parameter in SEDM, dimensionless                            |
| $N$        | = GLUE shape parameter, dimensionless                                  |
| $q$        | = gas production rate, MSCF/d  |
| $q_i$      | = initial production rate parameter in Hyperbolic model, MSCF/d        |
| $q_0$      | = initial production rate parameter in SEDM, MSCF/d                    |
| $P$        | = cumulative growth (production) in weibull model, MSCF                |
| $p$        | = instantaneous growth (production) in Weibull model, MSCF/d           |
| $w$        | = model weight based on GLUE approach, dimensionless                   |
| $\alpha$   | = scale parameter in Weibull model, d                                  |
| $\gamma$   | = shape parameter in Weibull model, dimensionless                      |
| $\sigma_o$ | = variance of observed values in GLUE approach, (MSCF) <sup>2</sup>    |
| $\sigma_e$ | = variance of errors (residuals) in GLUE approach, (MSCF) <sup>2</sup> |
| $\tau$     | = characteristic time parameter in SEDM, d                             |

## Acknowledgments

I thank Prof. John Lee for providing the Denton county data used in Example 2, and Battelle Memorial Institute for supporting this study through an internal research and development (IR&D) project.

## References

- Abramowitz, M. and Stegun, I.A. eds. 1972. Handbook of Mathematical Functions with Formulas, Graphs and Mathematical Tables, New York: Dover Publications.
- Arps, J.J. 1945. Analysis of Decline Curves. *Trans. AIME* **160**: 228-247.
- Blasingame, T.A. and Rushing, J.A. 2005. A Production-Based Method for Direct Estimation of Gas-in-Place and Reserves. Paper SPE

- 98042 presented at the SPE Eastern Regional Meeting, Morgantown, West Virginia, 14-16 September.
- Beven, K.J. and Binley, A. 1992. The Future of Distributed Models: Model Calibration and Uncertainty Prediction. *Hydrological Processes*, **6**: 279-298.
- Clark, A.J. 2011. Decline Curve Analysis in Unconventional Resource Plays using the Logistic Growth Model. MS Thesis, Department of Petroleum and Geosystems Engineering, The University of Texas at Austin.
- Duong, A.H. 2011. Rate-Decline Analysis for Fracture-Dominated Shale Reservoirs. SPEREE (June): 377-387.
- Fetkovich, M.J., Vienot, M.E., Bradley, M.D. and Kiesow, U.G. 1987. Decline Curve Analysis using Type Curves: Case Histories. *SPEFE* **2**(4):636-657.
- Harrell, D.R., Hodgins, J.E. and Wagenhofer, T. 2004. Oil and Gas Reserves Estimates: Recurring Mistakes and Errors. Paper SPE 91069 presented at the SPE Annual Technical Conference and Exhibition, Houston, 26-29 September. et al., 2004
- Ilk, D., Perego, A.D., Rushing, J.A. and Blasingame, T.A., 2008. Exponential versus Hyperbolic Decline in Tight Gas Sands – Understanding the Origin and Implications for Reserves Estimates using Arps' Decline Curves. Paper SPE 116731 presented at the SPE Annual Technical Conference and Exhibition, Denver, Colorado, 21-24 September.
- Kamal, M. 2009. Transient Pressure Analysis. SPE Monograph 35. Society of Petroleum Engineers, Richardson, TX.
- Kingland, S. 1982. The Refractory Model: The Logistic Curve and History of Population Ecology. *Quarterly Reviews in Biology* **57**: 29-51.
- Lee, W.J. and Sidle, R. 2010. Gas Reserves Estimation in Resource Plays. *SPE Economics & Management* (October): 86-91.
- Lee, W.J. 2012. Estimating Reserves in Unconventional Resources. Unpublished SPE Webinar Notes, 23 February.
- Maley, S. 1985. The Use of Conventional Decline Curve Analysis in Tight Gas Well Applications. Paper SPE 13898 presented at the SPE Low Permeability Gas Reservoirs Symposium, Denver, March 19-22.
- Neuman, S.P. 2003. Maximum Likelihood Bayesian Averaging of Uncertain Model Predictions, *Stochastic Environmental Research & Risk Assessment* **17** (5): 291-305.
- Singh, A., Mishra, S., and Ruskauff, G. 2010. Model Averaging Techniques for Quantifying Conceptual Model Uncertainty. *Ground Water* **48** (5): 701-715.
- Tabatabai, M., Williams, D.K., and Bursac, Z. 2005. Hyperbolic Growth Models: Theory and Application. *Theoretical Biology and Medical Modeling* **2**:14.
- Valko, P.P. 2009. Assigning Value to Simulation in the Barnett Shale: A Simultaneous Analysis of 7000 Plus Production Histories and Well Completion Records. Paper SPE 119639 presented at the SPE Hydraulic Fracturing Technology Conference, The Woodlands, Texas, USA, 19-21 January.
- Weibull, W. 1951. A Statistical Distribution Function of Wide Applicability. *J. Appl. Mech.* **18**: 293-297.
- Zeide, B. 1993. Analysis of Growth Equations. *Forest Sci.* **39**: 594-616.

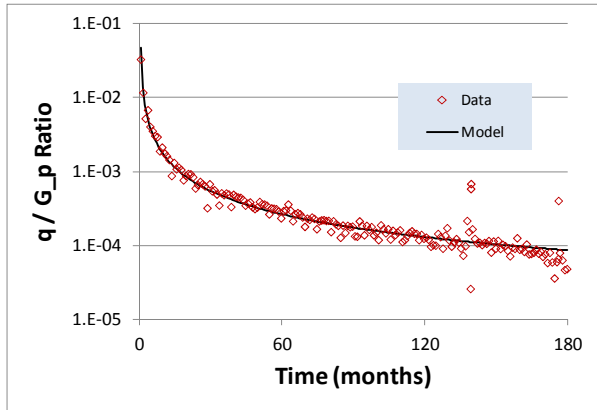


Figure 1 Example 1, Hyperbolic fit to  $q/G_p$  ratio.

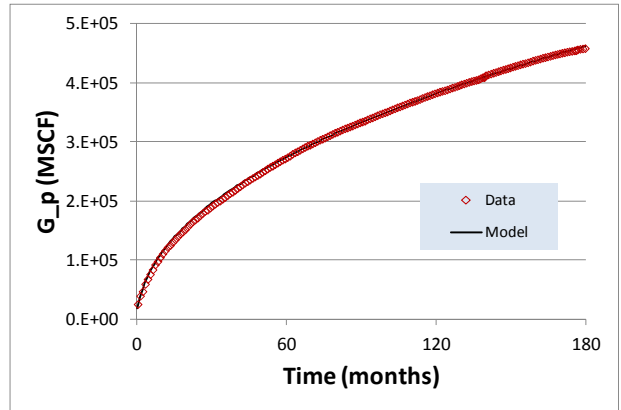


Figure 2 Example 1, Hyperbolic fit to  $G_p$  data.

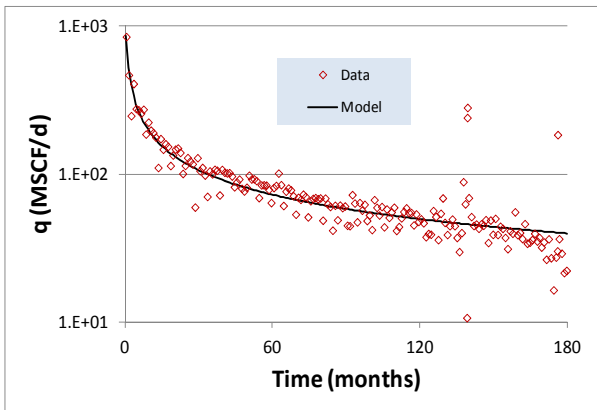


Figure 3 Example 1, Hyperbolic fit to  $q$  data.

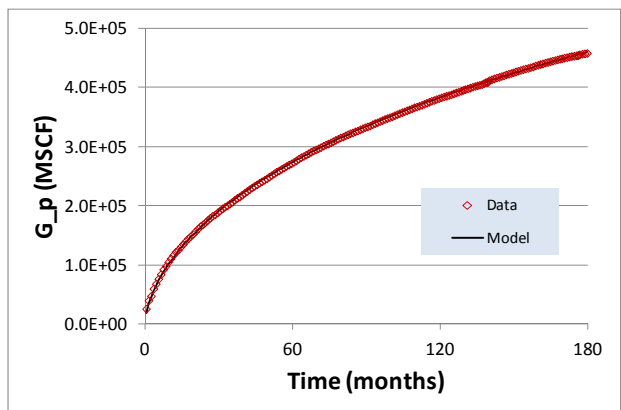


Figure 4 Example 1, SEDM fit to  $G_p$  data.

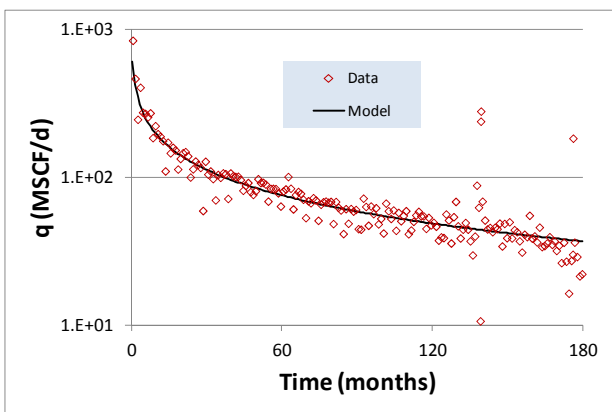


Figure 5 Example 1, SEDM fit to  $q$  data.

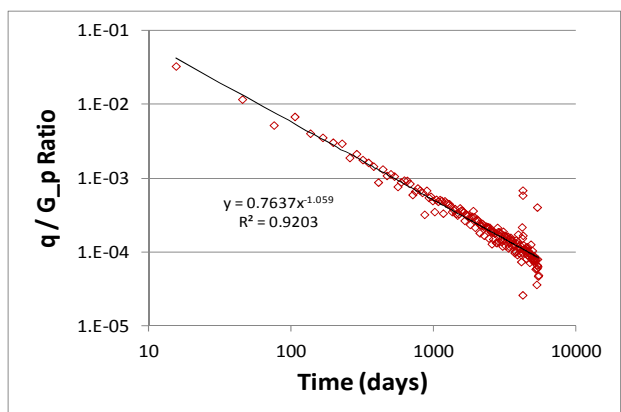


Figure 6 Example 1, Duong fit to  $q/G_p$  ratio.

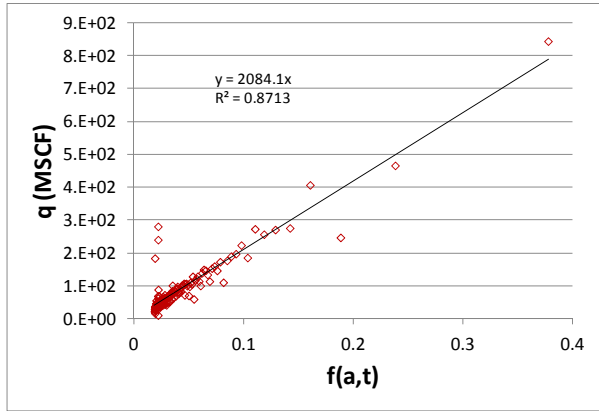


Figure 7 Example 1, Duong fit to  $q$  v/s  $f(a,t)$ .

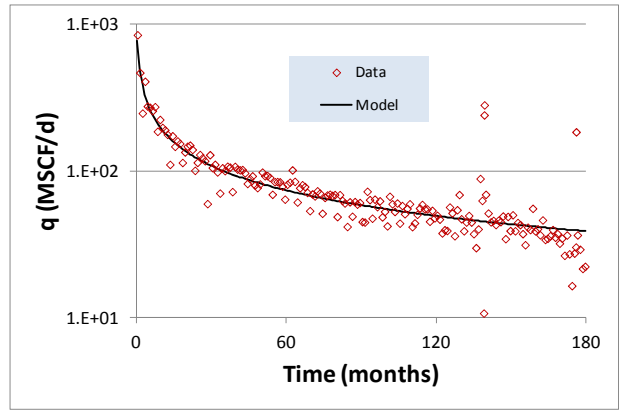


Figure 8 Example 1, Duong fit to  $q$  data.

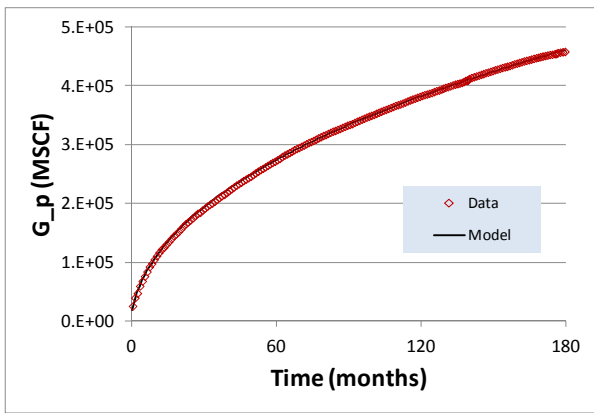


Figure 9 Example 1, Duong fit to  $G_p$  data

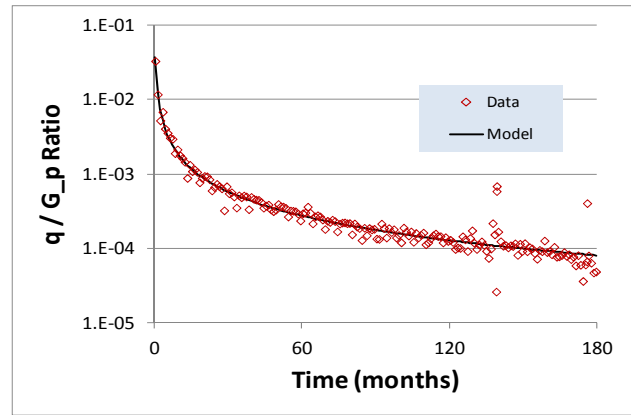


Figure 10 Example 1, Weibull fit to  $q/G_p$  ratio

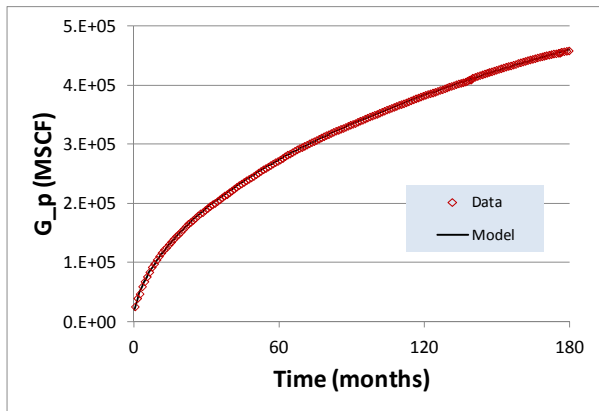


Figure 11 Example 1, Weibull fit to  $G_p$  data.

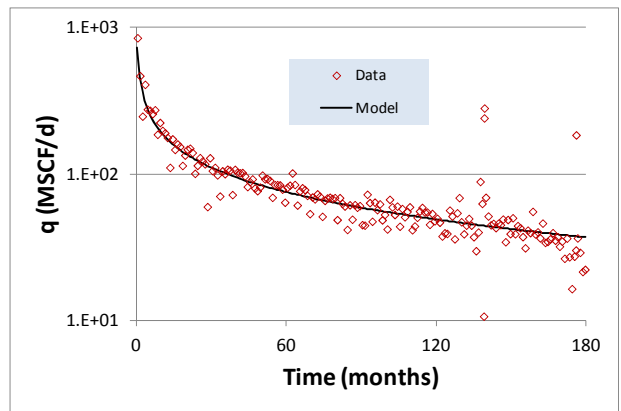


Figure 12 Example 1, Weibull fit to  $q$  data.

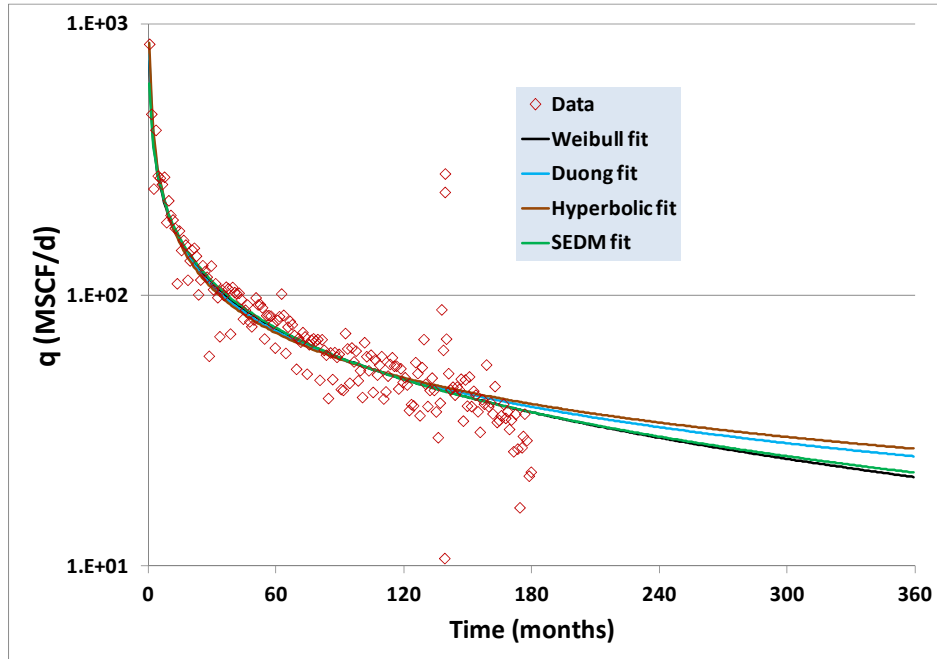


Figure 13 Example 1, comparison of 30-year forecasts for  $q$

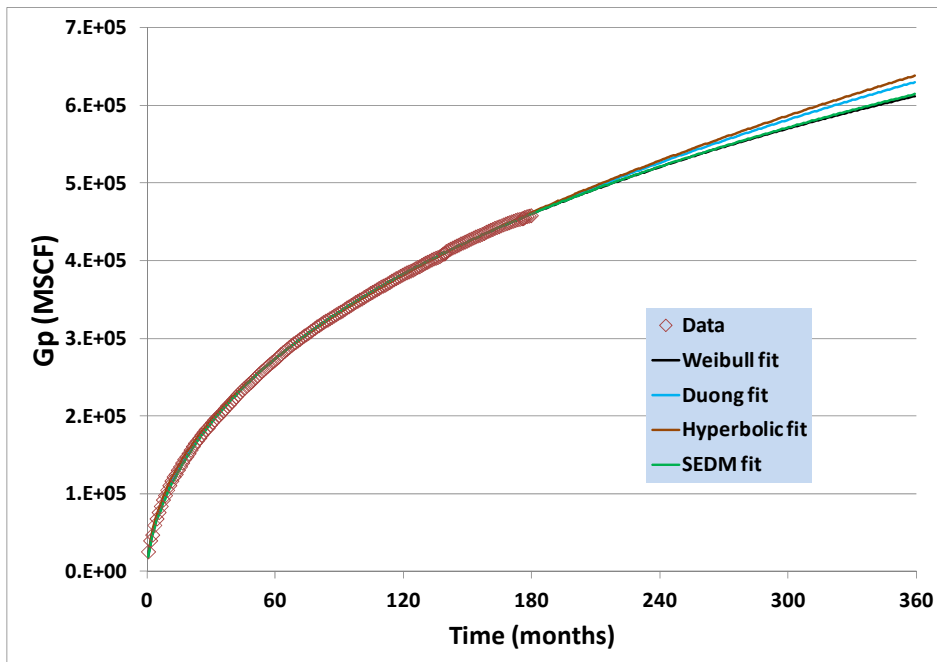


Figure 14 Example 1, comparison of 30-year forecasts for  $G_p$

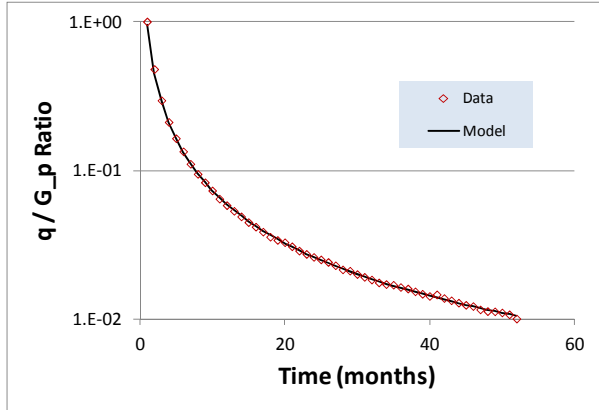


Figure 15 Example 2, Hyperbolic fit to  $q/G_p$  ratio

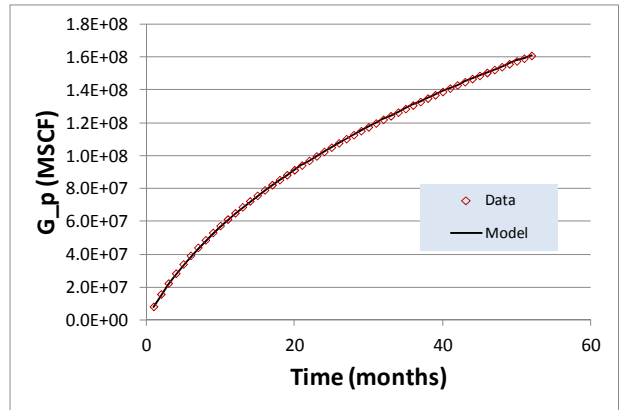


Figure 16 Example 2, Hyperbolic fit to  $G_p$  data

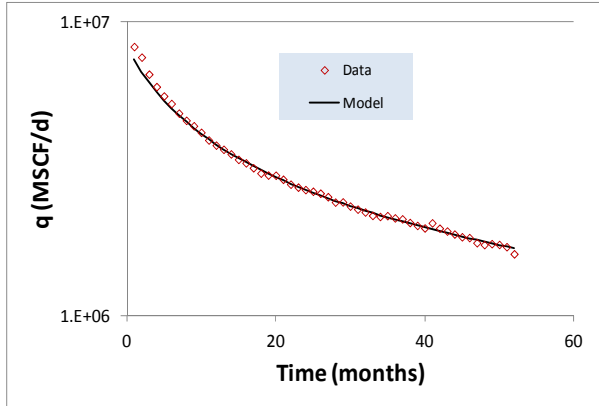


Figure 17 Example 2, Hyperbolic fit to  $q$  data

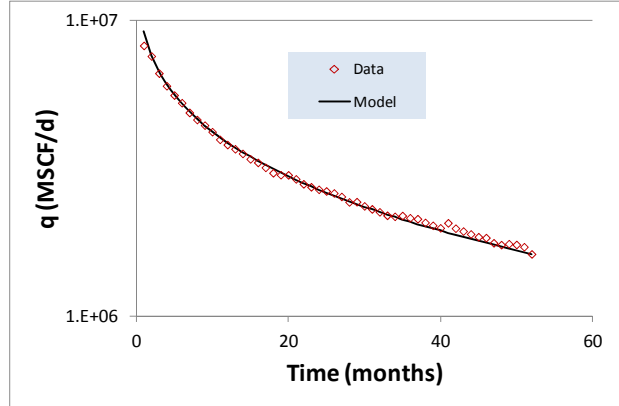


Figure 18 Example 2, SEDM fit to  $q$  data

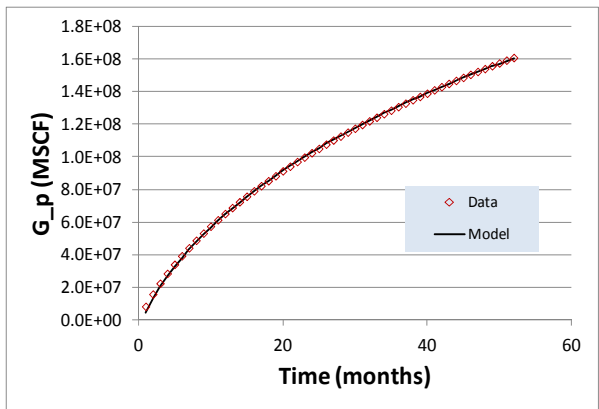


Figure 19 Example 2, SEDM fit to  $G_p$  data

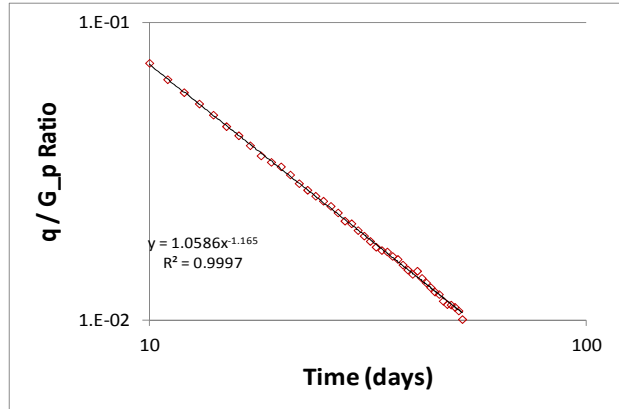


Figure 20 Example 2, Duong fit to  $q/G_p$  ratio

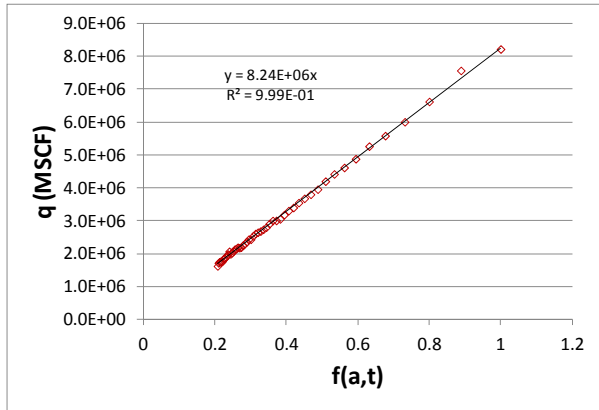


Figure 21 Example 2, Duong fit to  $q$  v/s  $f(a,t)$

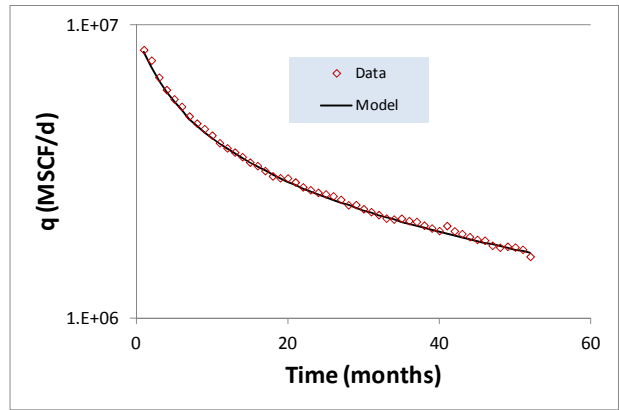


Figure 22 Example 2, Duong fit to  $q$  data

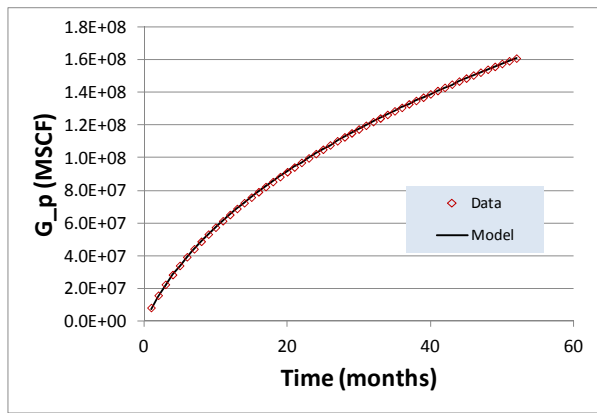


Figure 23 Example 2, Duong fit to  $G_p$  data

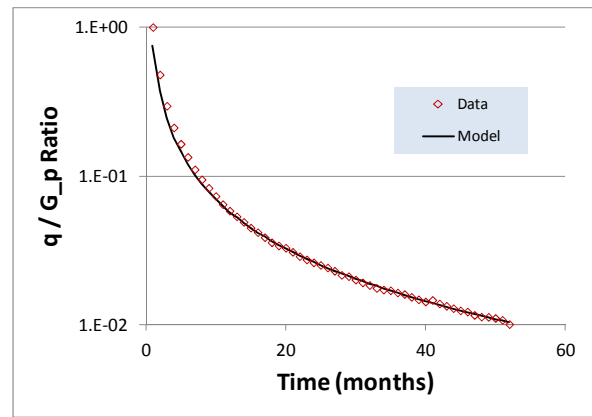


Figure 24 Example 2, Weibull fit to  $q/G_p$  ratio

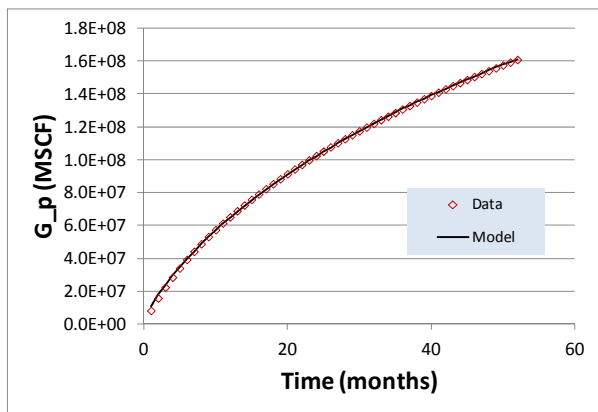


Figure 25 Example 2, Weibull fit to  $G_p$  data

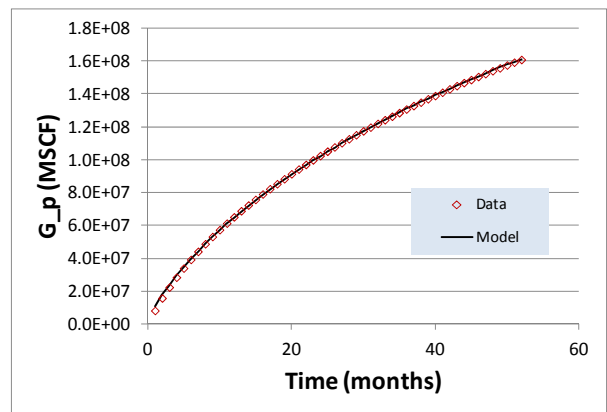


Figure 26 Example 2, Weibull fit to  $q$  data

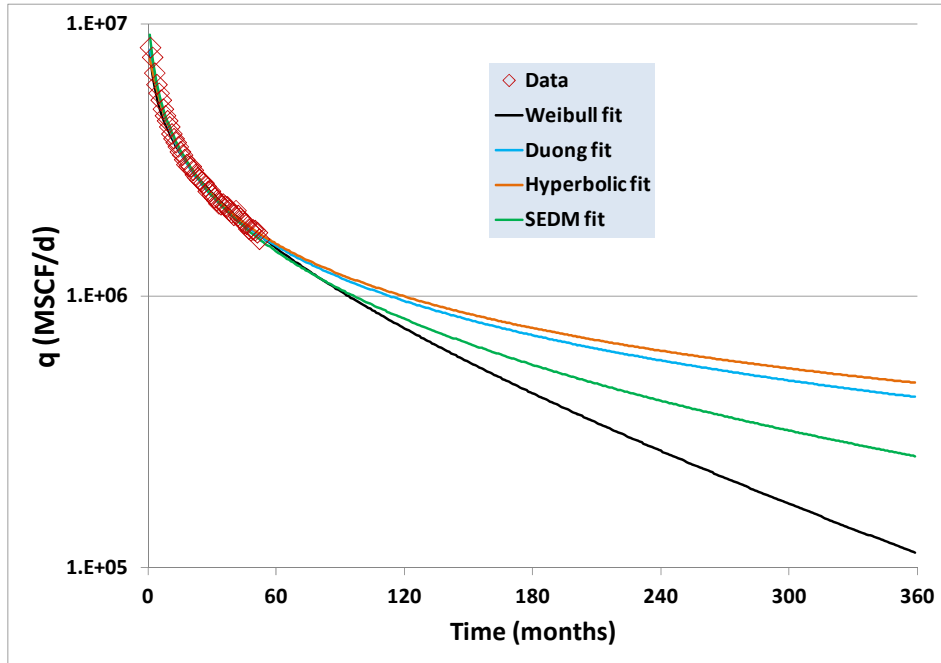


Figure 27 Example 2, comparison of 30-year forecasts for  $q$

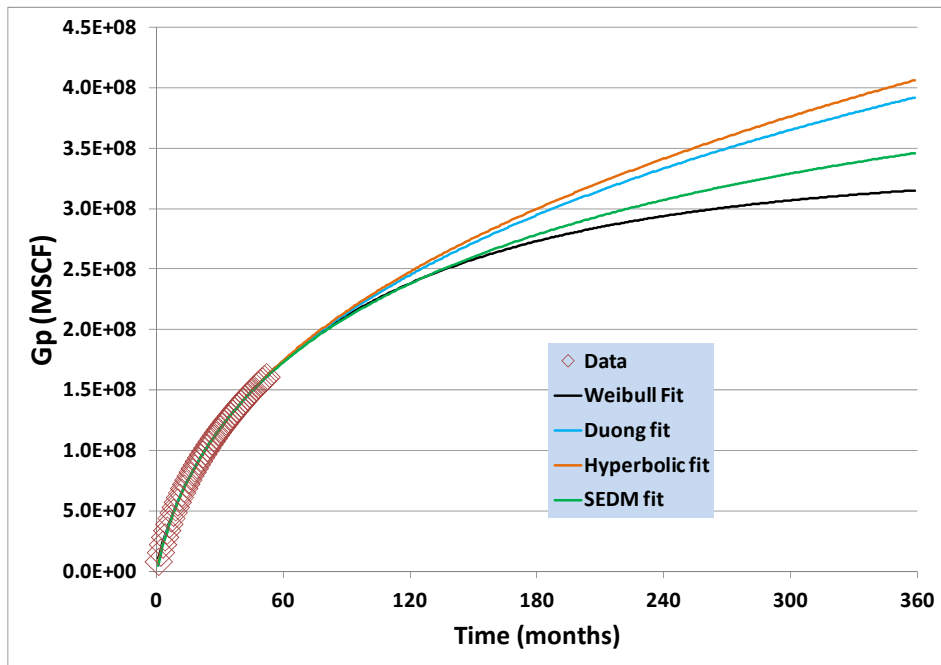


Figure 28 Example 2, comparison of 30-year forecasts for  $G_p$